JOURNAL OF COMPUTATIONAL BIOLOGY
Volume 27, Number 0, 2020

Pp. 1–13
DOI: 10.1089/cmb.2019.0265

Research Article

Solution of Ion Channel Flow Using Immersed Boundary–Lattice Boltzmann Methods

KUMAR SAURABH,[1,2] MAXIM SOLOVCHUK,[2] and TONY WEN HANN SHEU[1]

ABSTRACT

Poisson–Nernst–Planck (PNP) model has been extensively used for the study of channel flow under the influence of electrochemical gradients. PNP theory is a continuum description of ion flow where ionic distributions are described in terms of concentrations. Nonionic interparticle interactions are not considered in this theory as in continuum framework, their impact on the solution is minimal. This theory holds true for dilute flows or flows where channel radius is significantly larger than ion radius. However, for ion channel flows, where channel dimensions and ionic radius are of similar magnitude, nonionic interactions, particularly related to the size of the ions (steric effect), play an important role in defining the selectivity of the channel, concentration distribution of ionic species, and current across the channel, etc. To account for the effect of size of ions, several modifications to PNP equations have been proposed. One such approach is the introduction of Lennard-Jones potential to the energy variational formulation of PNP system. This study focuses on understanding the role of steric effect on flow properties. To discretize the system, Lattice Boltzmann method has been used. The system is defined by modified PNP equations where the steric effect is described by Lennard-Jones potential. In addition, boundary conditions for the complex channel geometry have been treated using immersed boundary method.

Keywords: immersed boundary method, ion-channel flow, Lattice Boltzmann method, steric effect.

1. INTRODUCTION

Transfer of bioions (Na^+, K^+, Ca^{2+}, and Cl^-) across the cell membrane is one of the most fundamental physiological processes. Bioion transport results in the generation and propagation of action potential in the neurons (Colbert and Pan, 2002), muscle contraction (Kuo and Ehrlich, 2015), conversion of light to electric signals in photoreceptors, and so on. Several specialized structures have evolved to ensure the movement of ions across the membrane and ion channels form a subset of these structures. Ion channels are embedded across the cell membrane and constitute a hydrophilic environment. Theoretical study of ion channels can be segregated into three different categories: (1) closing and opening of the ion channels (gating mechanism), (2) selectivity of ions, and (3) permeability.

Based on their gating mechanisms, ion channels can be broadly categorized into voltage-gated, ligand-gated (neurotransmitter), and lipid-gated channels. Other gating mechanisms such as the ones found in

[1]Department of Engineering Science and Ocean Engineering, National Taiwan University, Taipei, Taiwan.
[2]Institute of Biomedical Engineering and Nanomedicine, National Health Research Institute, Zhunan, Taiwan.

mechanosensitive channels and light-gated channels are also present. This study is focused on exploring the dependence of selectivity of channel on size of the ions.

In biological simulations, ion channels have been studied using continuum models based on Poisson–Nernst–Planck (PNP) equations, Monte Carlo method, Brownian dynamics, and molecular dynamics. Continuum-based approaches have often been deemed inaccurate, when compared with other approaches, due to their simplified approximations of atomic properties of the channel and the solution (Sagui and Darden, 1999; Corry et al., 2000; Im and Roux, 2002). In contrast, continuum models have been shown to be more efficient in studying the averaged properties of the system.

Over the years, several modifications to the standard PNP equations have been proposed in the literature to counter the shortcomings of PNP model (Gillespie, 2008; Liu, 2009; Kurnikova et al., 1999; Eisenberg, 2010). Liu and his group (Sheng et al., 2008; Liu, 2009; Xu et al., 2012) pioneered energetic variational (EnVar) approach that describes the energy of the system as Helmholtz free energy of classical thermodynamics (Sagui and Darden, 1999). This enabled the inclusion of multi-physics models in traditional PNP system. Kurnikova with her group (Kurnikova et al., 1999; Graf et al., 2004; Kurnikova and Coalson, 2005) tackled the problem by resorting to density functional theory. Nonner and Eisenberg (1998), Nonner et al. (1998, 2000), and Boda et al. (2002) developed a simplified model for ions present in the bulk solution and inside the filter by incorporating the effect of the size of ionic species. In their further research, they successfully showed that selectivity of certain types of ion channels can be explained with their model. This approach was further generalized by Eisenberg (2010), Eisenberg et al. (2010a,b, 2011), Hyon et al. (2011), Mori et al. (2011), and Horng et al. (2012) by adopting the EnVar approach. A detailed review of these mathematical models can be found in Chen and Wei (2016). In this study, we follow the methodology proposed in Horng et al. (2012). However, we are performing a 2D analysis as opposed to 1D analysis performed therein.

In this study, we solve for a 2D ion-channel flow using Lattice Boltzmann method (LBM). To address complex channel geometry, immersed boundary method (IBM) has been used ensuring the proper implementation of boundary conditions. The outline of the article is as follows. Basic mathematical model for standard and modified PNP equations is covered in Section 2. Furthermore, a brief introduction of LBM, in the context of PNP equations has also been provided. In Section 3, methodology to implement IBM for no-flux boundary conditions, with regard to Nernst–Planck equation, is discussed. Section 4 covers numerical validation of the scheme. Conclusion is provided in Section 5.

2. MATHEMATICAL MODELS

2.1. PNP equation

The PNP model is a well-established model for the study of ion transport. The model is constituted by

$$-\nabla.(\epsilon\nabla\phi) = \rho_0 + \sum_{i=1}^{N} z_i e c_i \tag{1a}$$

$$\frac{\partial c_i}{\partial t} + \nabla.J_i = 0, \qquad i = 1, \ldots, N \tag{1b}$$

$$J_i = -D_i(\nabla c_i + \frac{z_i e}{K_B T} c_i \nabla\phi), \tag{1c}$$

where ϵ is the dielectric constant, ϕ is the electrostatic potential, and ρ_0 is the fixed charge density. Poisson Equation (1a) describes the electrostatic potential field for the provided charge distributions. As for the Nernst–Planck Equation (1b), it describes the evolution of concentration of ionic species under the influence of electrochemical gradient. In Equation (1c), c_i represents the concentration, J_i represents the ionic flux, D_i represents diffusivity, z_i represents valency, e is the elementary charge, K_B is the Boltzmann constant, and T is the temperature. Please note that subscript ''i'' stands for the ith ionic species. Inclusion of steric effect results in the modification of the flux term in the NP equation.

$$J_i = -D_i(\nabla c_i + \frac{z_i e}{K_B T} c_i \nabla\phi + c_i \sum_{j=1}^{N} g_{ij} \nabla c_j), \tag{2}$$

where g_{ij} are the coefficients dependent on the size of the constituent ions. A detailed derivation can be found in Horng et al. (2012) and the references therein.

2.2. Lattice Boltzmann method

LBM is derived from the mesoscopic description of flow based on kinetic theory. In this study, instead of solving PNP, we essentially solve $N+1$ Boltzmann equations, one for Poisson equation, whereas the rest representing N Nernst–Planck equations. Boltzmann equation is given by

$$\frac{\partial f}{\partial t} + \mathbf{e}\frac{\partial f}{\partial \mathbf{x}} = \Omega(f), \tag{3}$$

where f is the density distribution function, $\mathbf{e}$ is the lattice velocity, and $\Omega(f)$ is the collision operator. Upon discretization, Equation (3) can be rewritten as

$$f_\alpha(\mathbf{x}+\mathbf{e}_\alpha\Delta t, t+\Delta t) = f_\alpha(\mathbf{x}, t) + \Delta t\Omega(f(\mathbf{x}, t)). \tag{4}$$

The collision operator can be approximated by Bhatnagar-Gross-Krook (BGK) operator (Bhatnagar et al., 1954) and Equation (4) can be simplified to

$$f_\alpha(\mathbf{x}+\mathbf{e}_\alpha\Delta t, t+\Delta t) = f_\alpha(\mathbf{x}, t) + \frac{1}{\tau}(f_\alpha^{eq}(\mathbf{x}, t) - f_\alpha(\mathbf{x}, t)). \tag{5}$$

In this study, α represents the lattice direction and τ is the relaxation parameter. For this study we are considering a D2Q9 lattice, that is, $\alpha = 0, \ldots, 8$.

For Poisson equation, the equivalence between mesoscopic and macroscopic properties is established through the following relations:

$$\phi = \sum_\alpha f_\alpha^P \tag{6a}$$

$$f_\alpha^{eq} = w_\alpha\phi. \tag{6b}$$

Similarly, defining a set of distribution functions for ion concentration such that

$$c_i = \sum_\alpha f_{\alpha,i}^{NP} \tag{7a}$$

$$f_{\alpha,i}^{eq} = w_\alpha c_i\left(1 + \frac{e_\alpha . V_{eff}}{c_s^2}\right) \tag{7b}$$

lead to Nernst–Planck equations, where c_s represents the velocity of sound and $V_{eff} = -D_i\frac{z_i e}{K_B T}\nabla\phi$.

2.3. Geometry and boundary conditions

For this study, we are considering the same geometry as in Horng et al. (2012). The channel Schematically shown in Figure 1 is 50 Å long and the width varies with the channel length. The maximum width has been taken as 80 Å and the filter region lies between 20 and 30 Å along the channel axis.

Radius of the channel varies as a function given by

$$r(z) = \frac{r_{\max} - r_{\min}}{(a/2)^{2p}}\left(z - \frac{a}{2}\right)^{2p} + r_{\min}, \tag{8}$$

where z is the location in the axial direction, $r(z)$ is the radius of channel at z, $r_{\max} = 40$ Å, $r_{\min} = 3.5$ Å, $a = 50$ Å, $p = 4$, and width $= 2r(z)$.

The system is represented by Equation (5), whereas the equilibrium distribution function is represented by Equations (6b) and (7b) for Poisson and Nernst–Planck equations, respectively. To obtain the dimensionless form of the governing equations, we adopt the following nondimensionalization parameters:

$$\tilde{c}_i = \frac{c_i}{c_{\mathrm{Na,\,max}}}, \qquad \tilde{\phi} = \frac{\phi}{K_B t/e}, \qquad \tilde{V} = \frac{V}{K_B T}$$

$$\tilde{s} = \frac{s}{L_{\mathrm{ref}}}, \qquad \tilde{t} = \frac{t}{L_{\mathrm{ref}}^2/D_{\mathrm{Na}}}, \qquad \tilde{D}_i = \frac{D_i}{D_{\mathrm{Na}}}$$

$$L_{\mathrm{ref}} = r_{\min}$$

For this study, bulk concentration is assumed to be constant. This assumption will lead to constant c_i and by extension, constant ϕ boundary conditions at the left, and right ends of the channel.

$$\phi(0)=\phi_0(0); \quad \phi(L)=\phi_0(L) \tag{10a}$$

$$c_{i,t}(0)=c_{i,0}(0); \quad c_{i,t}(L)=c_{i,0}(L) \tag{10b}$$

Please note that we are considering four ionic species Na^+, Ca^{2+}, Cl^-, and $CO^{0.5-}$. In Equation (10b), ''i'' represents Na^+, Ca^{2+}, and Cl^- as they are distributed in the whole domain. Since $CO^{0.5-}$ is confined to the filter region, $CO^{0.5-}$ must satisfy the no-flux condition at the boundary of the filter. To confine $CO^{0.5-}$ inside the filter, we introduce a restricting potential that can be expressed as

$$V=V_{\max}\gamma(z-0.5l)^2,$$

where γ is defined in a way that $V=V_{\max}$ on either end of the filter. This further leads to the modification of Nernst–Planck equation for $CO^{0.5-}$

$$J_i=-D_i(\nabla c_i+\frac{z_i e}{K_B T}c_i\nabla\phi+\frac{c_i}{K_B T}\nabla V).$$

Boundary conditions are shown in Figure 2.

For LBM, we transform the boundary conditions in terms of distribution functions.

$$f_\alpha^P(0)=2w_\alpha\phi_0(0)-f_{-\alpha}^P(0); \quad f_\alpha^P(0)=2w_\alpha\phi_0(L)-f_{-\alpha}^P(L) \tag{11a}$$

$$f_{i,\alpha}^{NP}(0)=2w_\alpha c_{i,0}(0)-f_{i,-\alpha}^{NP}(0); \quad f_{i,\alpha}^{NP}(L)=2w_\alpha c_{i,0}(L)-f_{i,-\alpha}^{NP}(L). \tag{11b}$$

α is the direction of the unknown component of distribution function, whereas $-\alpha$ is the opposite direction.

At the channel–membrane interface, Neumann boundary condition for Poisson equation and no-flux boundary condition for Nernst–Planck equations have to be satisfied. In Poisson equation, for the implementation of jump condition at membrane–channel interface, matched interface, and boundary method (Zhu et al., 2006; Pan et al., 2010; Zheng and Wei, 2011) has been used, whereas for no-flux boundary condition in Nernst–Planck equation, a methodology falling within the immersed boundary framework has been used. Details of its implementation are discussed next.

2.3.1. Immersed boundary method. IBM was developed by Peskin (1977) for the simulation of blood flow in heart. Since then, there have been a number of refinements and modifications. A detailed review can be found in Mittal and Iaccarino (2005). In this study, for a proper implementation of no-flux boundary condition for the Nernst–Planck equation we follow the methodology proposed in Shu et al. (2013). The boundary conditions are given as

$$(\nabla c_i^B+z_i c_i^B\nabla\phi^B).\mathbf{n}=0 \quad \text{standard PNP} \tag{12a}$$

$$(\nabla c_i^B+z_i c_i^B\nabla\phi^B+\sum_{j=1}^{N}c_i^B g_{ij}\nabla c_j^B).\mathbf{n}=0 \quad \text{modified PNP,} \tag{12b}$$

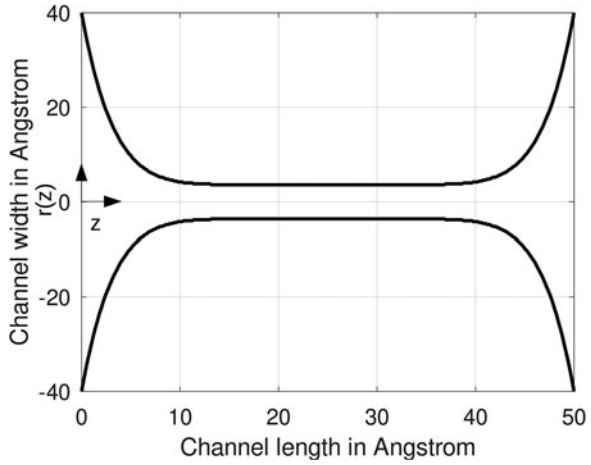

FIG. 1. Schematic of the channel.

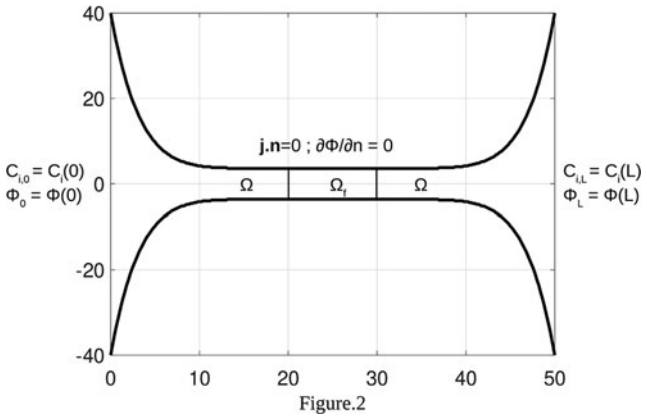

FIG. 2. Boundary conditions.

where **n** is the vector normal to the interface. To represent the effect of immersed boundary, we modify the Nernst–Planck equations to

$$\frac{\partial c_i}{\partial t} + \nabla . J_i = f \tag{13a}$$

$$f_\alpha(\mathbf{x} + \mathbf{e}_\alpha \Delta t, t + \Delta t) = f_\alpha(\mathbf{x}, t) + \frac{1}{\tau}(f_\alpha^{eq}(\mathbf{x}, t) - f_\alpha(\mathbf{x}, t)) + F_\alpha \Delta t, \tag{13b}$$

where f represents the forcing term due to the presence of immersed boundary. To calculate the forcing term, fractional step methodology has been implemented. To illustrate implementation steps, we are using standard PNP as an example. Extension to PNP-steric equation is straight forward. For the predictor step Equation (1b) can be solved using LBM to obtain the intermediate concentration value represented by c_i^*. This process can be represented as

- **Collision step**: $f_\alpha^*(\mathbf{x}, t) = f_\alpha(\mathbf{x}, t) + \frac{1}{\tau}(f_\alpha^{eq}(\mathbf{x}, t) - f_\alpha(\mathbf{x}, t))$
- **Streaming step**: $f_\alpha(\mathbf{x} + c_i \Delta t, t^*) = f_\alpha^*(\mathbf{x}, t)$
- **Flow variable calculation**: $c_i^*(\mathbf{x}) = \sum_\alpha f_\alpha(\mathbf{x}, t^*)$.

Next we calculate normal flux at the boundary, Equation (12a). To obtain normal flux, we have to calculate intermediate concentration and gradients of intermediate concentration and potential at the boundary. We use delta function for their calculation. The process can be represented as

$$\frac{\partial c_i^*(\mathbf{x})}{\partial x} = \frac{c_i^{*,j+1,k} - c_i^{*,j-1,k}}{2\Delta x}; \quad \frac{\partial c_i^*(\mathbf{x})}{\partial y} = \frac{c_i^{*,j,k+1} - c_i^{*,j,k-1}}{2\Delta y}$$

$$\frac{\partial \phi(\mathbf{x})}{\partial x} = \frac{\phi^{j+1,k} - \phi^{j-1,k}}{2\Delta x}; \quad \frac{\partial \phi(\mathbf{x})}{\partial y} = \frac{\phi^{j,k-1} - \phi^{j,k-1}}{2\Delta y}$$

$$\nabla c_i^{*,B} = \sum_{\mathbf{x}=1}^{4} \delta_{B\mathbf{x}_i} \left(\frac{\partial c_i^*(\mathbf{x})}{\partial x} + \frac{\partial c_i^*(\mathbf{x})}{\partial y} \right)$$

$$\nabla \phi^B = \sum_{\mathbf{x}=1}^{4} \delta_{B\mathbf{x}_i} \left(\frac{\partial \phi(\mathbf{x})}{\partial x} + \frac{\partial \phi(\mathbf{x})}{\partial y} \right)$$

$$c_i^{*,B} = \sum_{\mathbf{x}=1}^{4} \delta_{B\mathbf{x}} c_i^*(\mathbf{x})$$

Delta function is calculated as

$$\delta_{B\mathbf{x}_i} = \begin{cases} \left(1 - \frac{|x_B - x_i|}{\Delta x}\right)\left(1 - \frac{|y_B - y_i|}{\Delta y}\right), & \text{if } |x_B - x_i| < \Delta x \text{ and } |y_B - y_i| < \Delta y \\ 0, & \text{otherwise} \end{cases}$$

1, 2, 3, and 4 are the neighboring points such that $|x^B - x^i| < \Delta x$ and $|y^B - y^i| < \Delta y$ for $i = 1, \ldots, 4$. Neighboring points corresponding to boundary point B are labeled clearly in Figure 3.

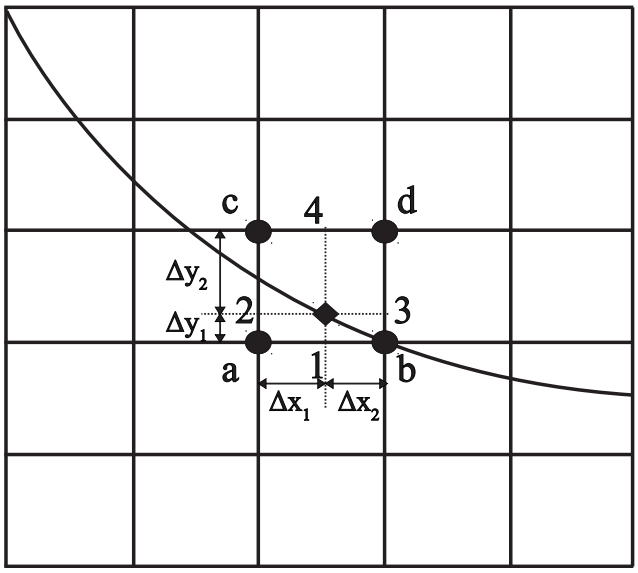

FIG. 3. A generalized schematic of membrane–channel interface. 1, 2, 3, and 4 represent the neighboring nodes, whereas B represents the boundary node.

Once we obtain the values of $c_i^{*,B}$, $\nabla c_i^{*,B}$, and $\nabla\phi^B$, we can calculate the normal flux at the boundary $fl^B = (\nabla c_i^B + z_i c_i^B \nabla\phi^B).\mathbf{n}$. In the corrector step, we assign a forcing term at the boundary such that the no-flux boundary condition is satisfied. This results in forcing term $= -fl^B$. Then we extrapolate this value to the neighboring nodes using delta function. In LBM frame the process can be described as

- **Collision**: $f_\alpha^*(\mathbf{x}, t^*) = f_\alpha(\mathbf{x}, t^*) + \frac{1}{\tau}(f_\alpha^{eq}(\mathbf{x}, t^*) - f_\alpha(\mathbf{x}, t^*)) + F_\alpha(\mathbf{x}, t)\Delta t$
- **Streaming**: $f_\alpha(\mathbf{x} + c_i\Delta t, t + \Delta t) = f_\alpha^*(\mathbf{x}, t^*)$

where $F_\alpha(\mathbf{x}, \mathrm{t}) = -\sum_{j,k} \delta_{Bjk} fl^B$.

3. NUMERICAL VALIDATION

In this study, we have analyzed the effect of steric term on the concentration distribution of ionic species in the channel. This analysis is an extension of the analysis performed in Horng et al. (2012) where the equations were solved in an axis-symmetric 1D framework. To validate our results, we have compared the concentration profiles along channel axis with their results and a significant match has been observed. For all the cases, we have fixed the potential as 100 mV on either side of the channel. Concentration of Na^+ ion is fixed at 100 mM on either side, whereas concentration of Ca^{2+} ion varies. Cl^- is kept at a concentration to make the bulk solution electrically neutral. $CO^{0.5-}$ concentration acquires the value equivalent to four carboxyl groups and it is distributed uniformly inside the filter. The maximum value of nondimensionalized restricting potential is kept at 200. Diffusion coefficients (m^2/s) in bulk solution are $D_{Na} = 1.334 \times 10^{-9}$, $D_{Ca} = 0.792 \times 10^{-9}$, $D_{Cl} = 2.032 \times 10^{-9}$, and $D_{CO} = 0.76 \times 10^{-9}$. In the filter region, diffusion coefficients are set to 1/20th of their bulk values. Dielectric constant is $80\epsilon_0$ in the bulk solution, whereas it takes a value of $30\epsilon_0$ inside the filter. In membrane region, we assign it a value of $2\epsilon_0$.

In the first case, we are reporting the impact of increasing the steric effect on the centreline concentration profile. The coefficient values are listed in Table 1. Concentration of Ca^{2+} is fixed at 1×10^{-3} M on either side of the channel.

TABLE 1. DIFFERENT SET OF COEFFICIENTS OF STERIC TERMS

g_{NaNa}	0	10^{-4}	10^{-2}
g_{NaCa}	0	6.41×10^{-5}	6.41×10^{-3}
g_{NaO}	0	8.19×10^{-4}	8.19×10^{-2}
g_{CaCa}	0	1.64×10^{-4}	1.64×10^{-2}
g_{CaO}	0	1.00×10^{-3}	1.00×10^{-1}
g_{OO}	0	1.64×10^{-2}	1.64

In PNP-steric equations, we model electrochemical and steric forces acting on ionic species. Electrochemical forces originate from ionic interactions and potential gradient. Depending upon the nature of interacting species, electrochemical forces could be attractive or repulsive in nature. Steric forces represent nonionic interactions and are typically repulsive for small distances. Thus, we have considered only the repulsive part of nonionic interactions in our model. In the absence of steric forces, one would expect that Na^+ and Ca^{2+} ions present in the bath, to get attracted toward anionic filter repelling each other at the same time, whereas Cl^- to be pushed away from the filter. Owing to high concentration of $CO^{0.5-}$ inside the filter, these interactions would result in the accumulation of cationic species inside the filter. This can be observed clearly in Figure 4a. Thus, for this study, accumulation of cationic species in the filter is a typical result of standard PNP model. Please note that an accumulation of carboxyl group toward the centre is significantly influenced by restricting potential and different restricting potential profiles will result in different concentration profiles.

Next we studied the impact of adding steric forces to the system. It is important to note that the ratio of steric terms for species is fixed; however, their absolute value is not. Thus, we have considered three different sets of values as shown in Table 1. Steric forces would introduce more repulsion, which would oppose the accumulation of ionic species inside the filter. As a result, maximum concentration inside the channel would drop and the profile would become flatter. The same behavior can be observed upon comparing Figure 4a and b, where Figure 4a is a solution of standard PNP. Owing to their different valency, Ca^{2+} experiences higher attraction toward the filter compared with Na^+. For sufficiently large steric coefficient values, repulsion forces for Na^+ could overcome the attraction forces and Na^+ ions would be pushed away from the centre of the filter toward the corners. This would result in creation of a depletion zone in the centre of the filter and accumulation toward the corners. The concentration profile that showed a single peak for previous cases will show two peaks near the corners. This is termed as the splitting of concentration profile. As expected, Ca^{2+} experiences further flattening of the concentration profile; however, concentration profile does not split. In Figure 4c, where $g_{NaNa} = 10^{-2}$, we can clearly observe this behavior.

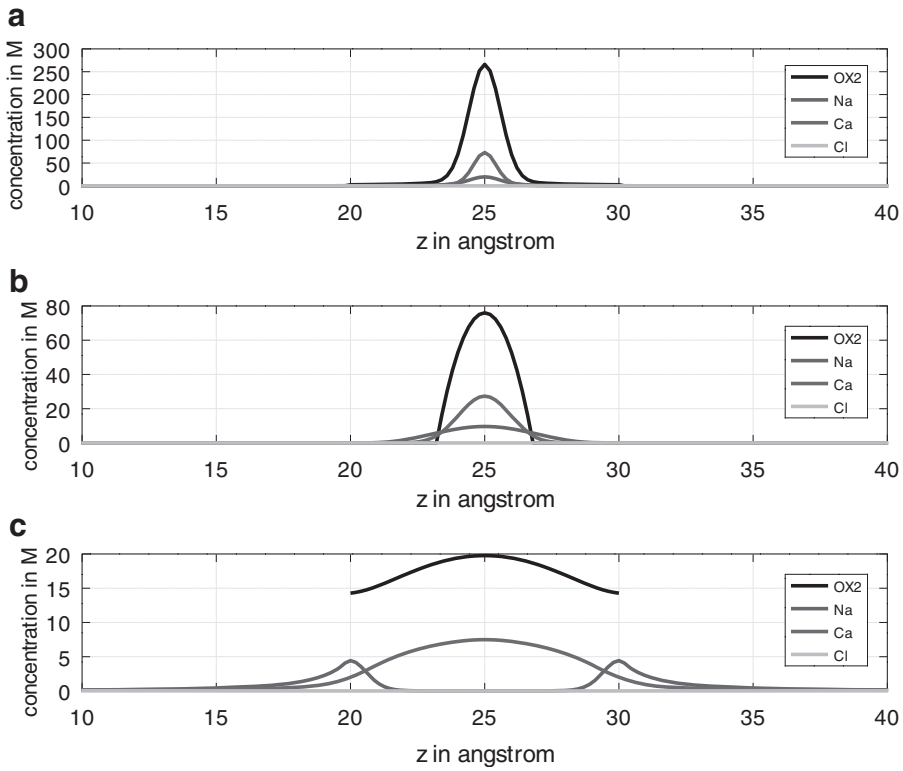

FIG. 4. Species concentration distributions for various g_{NaNa}. $V_{max} = 200$, $\phi_0 = \phi_L = 100\,mV$ and $Na_0^+ = Na_L^+ = 100$ mM, $Ca_0^{2+} = Ca_L^{2+} = 1$ mM. **(a)** $g_{NaNa} = 0$, **(b)** $g_{NaNa} = 10^{-4}$, and **(c)** $g_{NaNa} = 10^{-2}$. The results are in good agreement with the results published in Horng et al. (2012).

Figure 5 illustrates the impact of increasing the concentration of Ca^{2+} ion while keeping the concentration of Na^{+} at a fixed value in the absence of steric force. As the concentration of Ca^{2+} in the bath increases, more and more Ca^{2+} ions get accumulated inside the filter and the concentration profile adopts a Maxwellian distribution. It should be noted that in biological systems, Ca^{2+} concentration varies over a range of 1×10^{-8} to 1×10^{-2} M. Therefore, the bath concentration is a representative of realistic scenario. Although accumulation of Ca^{2+} increases with the increasing bath concentration, only at the moment when Ca^{2+} bath concentration reaches 10^{-4} M value, ionic concentration of both cationic species is comparable inside the filter.

Next, we introduced steric forces where $g_{\mathrm{NaNa}}=1\times10^{-2}$ and performed simulation for the same set of parameters and bulk concentrations. The results are illustrated in Figure 6.

In this study, we observe a significant drop in the concentrations of all species in the filter. As the concentration of Ca^{2+} in the bath increases, more Ca^{2+} are getting accumulated inside the filter, which increase both electrostatic and steric repulsions for Na^{+}. As a result, with increasing Ca^{2+}, we observe higher depletion in the concentration profile of Na^{+} ion in Figure 6. Similar to the previous case Figure 5, an increase in bath concentration leads to an increase in the concentration inside the filter. However, the concentrations of both the species become comparable for a much smaller Ca^{2+} bath concentration. This can be observed clearly from the binding curves shown in Figure 7 where binding ratio for calcium is defined as

$$\text{Binding ratio} = \frac{\text{No. } Ca^{2+} \text{ ions inside filter}}{\text{No. } Ca^{2+} \text{ ions inside filter} + \text{No. } Na^{+} \text{ ions inside filter}}.$$

Significant difference between the binding curves with and without steric term highlights the limitation of standard PNP model. Steric term greatly enhances the selectivity of Ca^{2+} ions. In addition, the binding curves match significantly with the ones published in Horng et al. (2012).

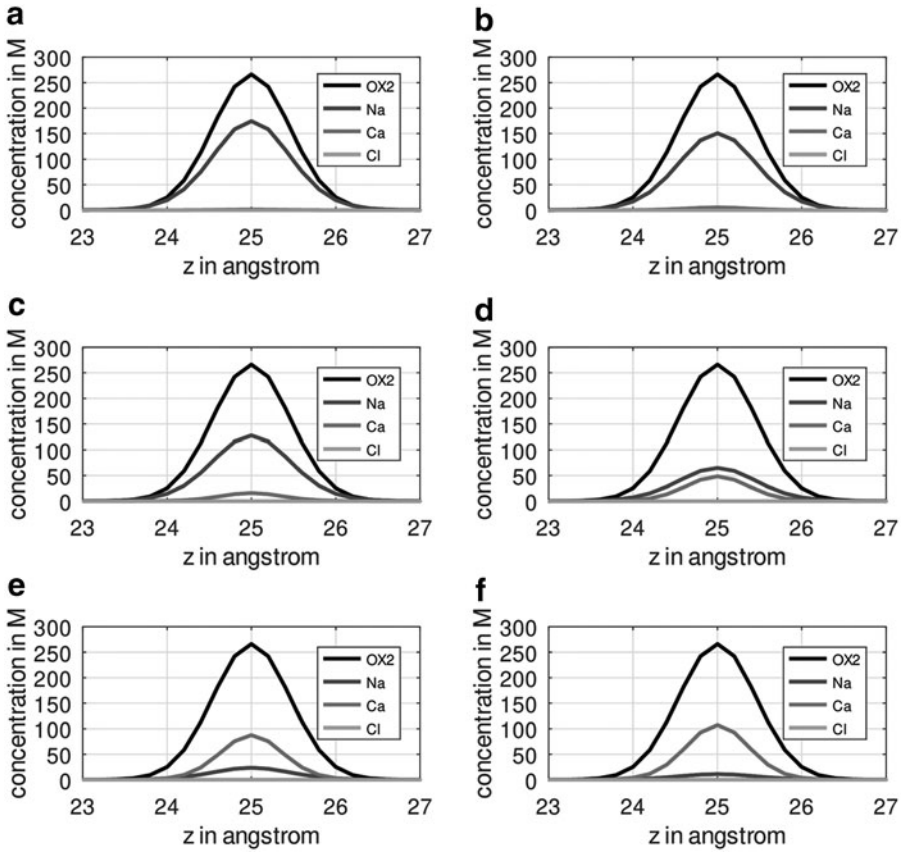

FIG. 5. Species concentration distributions at fixed Na^{+} bath concentration of 0.1 M and different Ca^{2+} bath concentrations. $V_{\max}=200$, $\phi_0=\phi_L=100$ mV, and $g_{\mathrm{NaNa}}=0$. **(a)** $Ca^{2+}=1\times10^{-7}$ M, **(b)** $Ca^{2+}=1\times10^{-6}$ M, **(c)** $Ca^{2+}=1\times10^{-5}$ M, **(d)** $Ca^{2+}=1\times10^{-4}$ M, **(e)** $Ca^{2+}=1\times10^{-3}$ M, and **(f)** $Ca^{2+}=1\times10^{-2}$ M. The results are in good agreement with the results published in Horng et al. (2012).

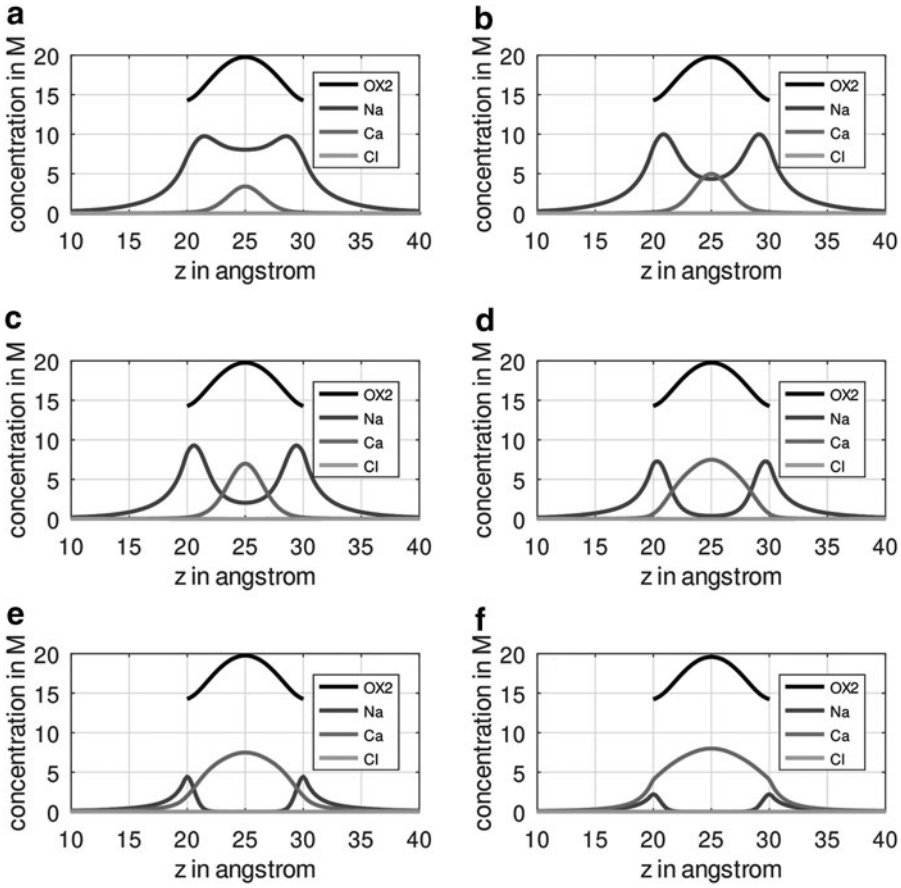

FIG. 6. Species concentration distributions at fixed Na^+ bath concentration of 0.1 M and different Ca^{2+} bath concentrations. $V_{max} = 200$, $\phi_0 = \phi_L = 100$ mV, and $g_{NaNa} = 0.01$. **(a)** $Ca_0^{2+} = Ca_L^{2+} = 10^{-7}$ M, **(b)** $Ca_0^{2+} = Ca_L^{2+} = 10^{-6}$ M, **(c)** $Ca_0^{2+} = Ca_L^{2+} = 10^{-5}$ M, **(d)** $Ca_0^{2+} = Ca_L^{2+} = 10^{-4}$ M, **(e)** $Ca_0^{2+} = Ca_L^{2+} = 10^{-3}$ M, and **(f)** $Ca_0^{2+} = Ca_L^{2+} = 10^{-2}$ M. The results are in good agreement with the results published in Horng et al. (2012).

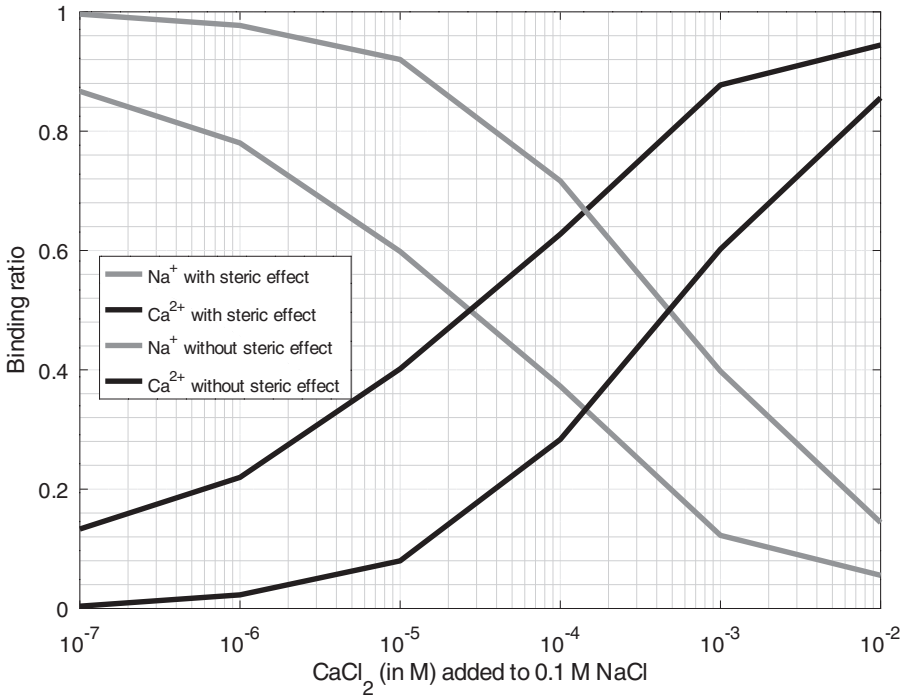

FIG. 7. The predicted binding curves with ($g_{NaNa} = 0.01$) and without ($g_{NaNa} = 0$) steric forces.

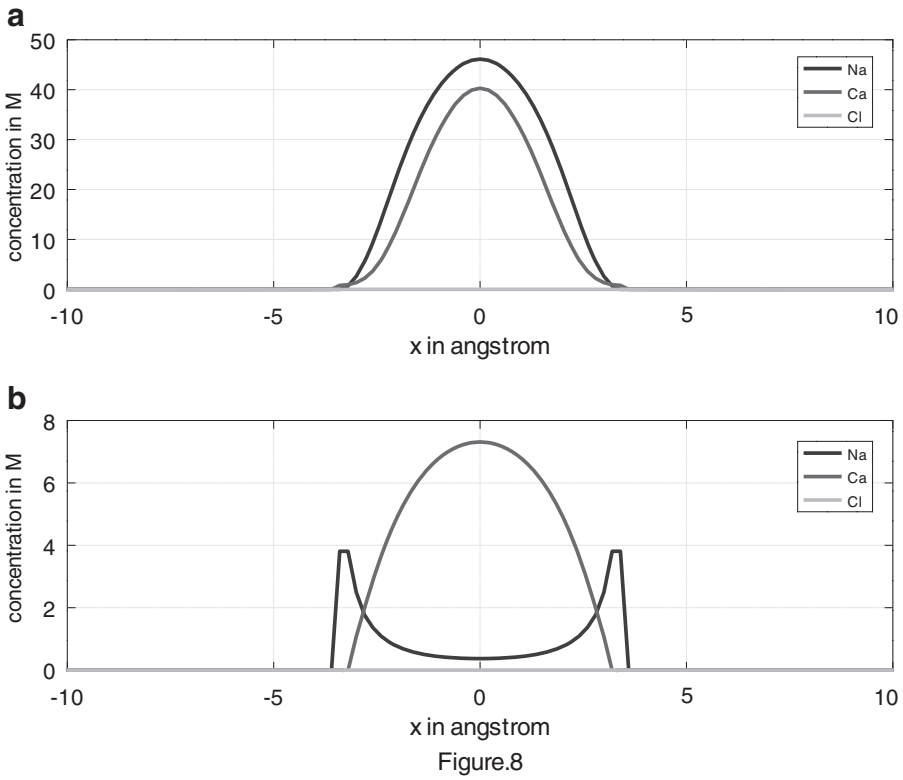

FIG. 8. Species concentration distributions in the direction perpendicular to the channel axis. $V_{\max} = 200$, $\phi_0 = \phi_L = 100\,\text{mV}$ and $\text{Na}_0^+ = \text{Na}_L^+ = 100\,\text{mM}$, $\text{Ca}_0^{2+} = \text{Ca}_L^{2+} = 1\,\text{mM}$. **(a)** $g_{\text{NaNa}} = 0$ and **(b)** $g_{\text{NaNa}} = 10^{-2}$.

To understand the effect of two dimensionality of the system we have plotted the concentration profiles in the direction perpendicular to the channel axis at half length of the channel. In Figure 8, in the absence of steric effect, we observe that the maximum concentration lies at centre of the channel, which is coincident with the channel axis, whereas at the channel–membrane interface the concentration is zero. As was observed along the channel axis, steric effect will oppose the accumulation of ionic species, pushing them toward the channel–membrane interface. As before, this would result in flattening of the concentration profile, this time along the direction of channel width. For $g_{\text{NaNa}} = 0.01$, we observed splitting in concentration profile of Na^+ ion thereby establishing two peaks near the channel–membrane interface.

So far we have discussed the role of steric repulsion in determining the ionic concentration distribution. Another factor that can significantly influence ionic distribution is the geometry of the channel. To illustrate this further, we are considering the channel where the selectivity filter is not cylindrical. Channel geometry is given in Figure 9. To avoid any influence from the steric repulsions, we are considering $g_{\text{NaNa}} = 0$. The results are plotted in Figure 10. Upon comparison with the previous nonsteric case, we observed an overall increase in the concentration of $CO^{0.5-}$. Thus, as the concentration of Ca^{2+} in the bath increases, higher concentration of Ca^{2+} will get accumulated at the centre of the filter. This will result in the channel becoming Ca^{2+} selective for a lower Ca^{2+} bath concentration. As the only difference between the current and the previous channel is the shape of the filter region, this increase must be an outcome of the reduction of minimum channel width.

4. CONCLUSION

In this article, we performed a 2D analysis of ion channel using EnVar approach-based PNP models. The system was descretized using LBM. For the complex boundary, we used no-flux boundary condition enforced IBM. There is a good match between our results and the ones available in literature. One of the key features of the steric term is to provide repulsion mechanism among ionic species that should eventually result in a splitting of concentration profile leading to the emergence of peaks in concentration near

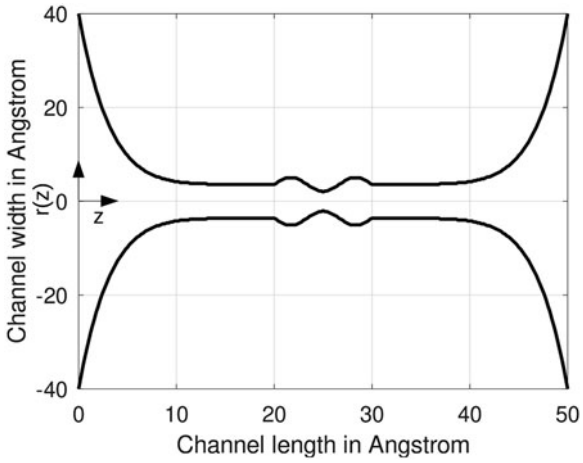

FIG. 9. Schematic of the new channel.

the corners of the filter and channel–membrane interface. In addition, we have successfully illustrated that filter geometry can significantly influence concentration profile.

Conclusively, steric repulsions and filter geometry play significant roles in defining the ionic distribution inside the channel. Thus, to obtain more accurate results for ion flows, it is very important to correctly define the coefficients for the steric term and to construct channel geometry more accurately. Furthermore, it is important to note that modified PNP-based analysis has been successful at replicating results based on noncontinuum models and is computationally inexpensive compared with its counterparts. Thus, it is

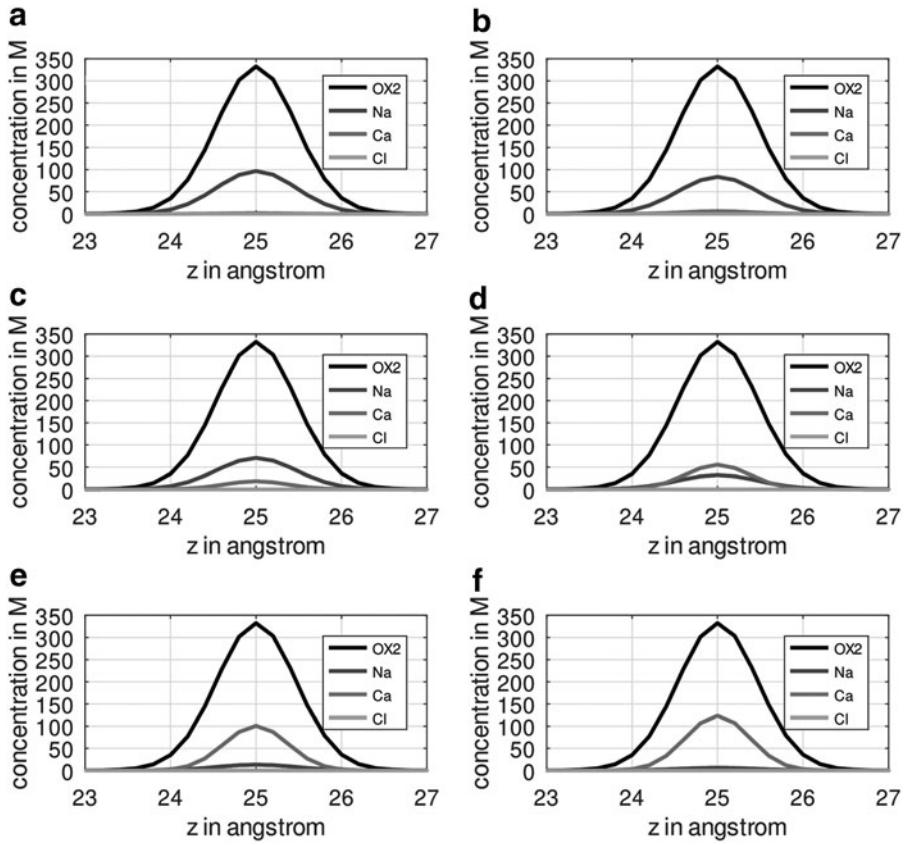

FIG. 10. Species concentration distributions for the cases at the fixed Na^+ bath concentration of 0.1 M under various Ca^{2+} bath concentration. **(a)** $Ca^{2+} = 1 \times 10^{-7}$ M, **(b)** $Ca^{2+} = 1 \times 10^{-6}$ M, **(c)** $Ca^{2+} = 1 \times 10^{-5}$ M, **(d)** $Ca^{2+} = 1 \times 10^{-4}$ M, **(e)** $Ca^{2+} = 1 \times 10^{-3}$ M, and **(f)** $Ca^{2+} = 1 \times 10^{-2}$ M.

worthwhile to investigate it further to make it more robust. To the best of authors' knowledge, this is the first time PNP-steric model, based on EnVaR approach, has been solved using LBM–IBM for a 2D ion channel.

AUTHOR DISCLOSURE STATEMENT

The authors declare they have no competing financial interests.

FUNDING INFORMATION

This study was supported in part by NHRI (National Health Research Institute, Institute of Biomedical Engineering and Nanomedicine, Zhunan, Taiwan, Project number BN-106-PP-08) and MOST (Ministry of Science and Technology, Taipei, Project number MOST-106-2115-M-400-001-) project.

REFERENCES

Bhatnagar, P.L., Gross, E.P., and Krook, M. 1954. A model for collision processes in gases. I. Small amplitude processes in charged and neutral one-component systems. *Phys. Rev.* 94, 511–525.

Boda, D., Busath, D., Nonner, W., et al. 2002. Monte Carlo simulations of ion selectivity in a biological Na channel: Charge–space competition. *Phys. Chem. Chem. Phys.* 4, 5154–5160.

Chen, D., and Wei, G.-W. 2016. A review of mathematical modeling, simulation and analysis of membrane channel charge transport. arXiv:1611.04573v1.

Colbert, C., and Pan, E. 2002. Ion channel properties underlying axonal action potential initiation in pyramid neuron. *Nat. Neurosci.* 5, 533–538.

Corry, B., Kuyucak, S., and Chung, S.H. 2000. Tests of continuum theories as models of ion channels. II. Poisson–Nernst–Planck theory versus Brownian dynamics. *Biophys. J.* 78, 2364–2381.

Eisenberg, B. 2010. Multiple scales in the simulation of ion channels and proteins. *J. Phys. Chem. C* 114, 20719–20733.

Eisenberg, B., Hyon, Y., and Liu, C. 2010a. Energy variational analysis of ions in water and channels: Field theory for primitive models of complex ionic fluids. *J. Chem. Phys.* 133, 104104.

Eisenberg, B., Hyon, Y., and Liu, C. 2011. A mathematical model for the hard sphere repulsion in ionic solutions. *Commun. Math. Sci.* 9dd, 459–475.

Eisenberg, R.S., Hyon, Y., and Liu, C. 2010b. Energetic variational analysis EnVarA of ions in calcium and sodium channels. *Biophys. J.* 98, 515a.

Gillespie, D. 2008. Energetics of divalent selectivity in a calcium channel: The ryanodine receptor case study. *Biophys. J.* 94, 1169–1184.

Graf, P., Kurnikova, M.G., et al. 2004. Comparison of dynamic lattice Monte Carlo simulations and the dielectric self-energy Poisson-Nernst-Planck continuum theory for model ion channels. *J. Phys. Chem.* 108, 2006–2015.

Horng, T.L., Lin, T.C., Liu, C., et al. 2012. PNP equation with steric effects: A model of ion flow through channels. *J. Phys. Chem.* 116, 11422–11440.

Hyon, Y., Foncesca, J., Eisenberg, R.S., et al. 2011. A new Poisson-Nernst-Planck equation (PNP-FS-IF) for charge inversion near walls. *Biophys. J.* 100, 578a.

Im, W., and Roux, B. 2002. Ion permeation and selectivity of OmpF porin: A theoretical study based on molecular dynamics, Brownian dynamics, and continuum electrodiffusion theory. *J. Mol. Biol.* 322, 851–869.

Kuo, I.Y., and Ehrlich, B.E. 2015. Signaling in muscle contraction. *Cold Spring Harb. Perspect. Biol.* 7, a006023.

Kurnikova, M.G., and Coalson, A. 2005. Poisson-Nernst-Planck theory approach to the calculation of current through biological ion channels. *IEEE Trans. Nanobioscience* 4, 81–93.

Kurnikova, M.G., Coalson, R.D., Graf, P., et al. 1999. A lattice relaxation algorithm for three-dimensional Poisson-Nernst-Planck theory with application to ion transport through the gramicidin A channel. *Biophys. J.* 76, 642–656.

Liu, C. 2009. An introduction of elastic complex fluids: an energetic variational approach, 286–337. *In* Hou, Y.T., Liu, C. and Liu, J.-G., eds. *Multi-Scale Phenomenon in Complex Fluids: Modeling, Analysis and Numerical Simulations*. World Scientific Publishing Company, Singapore.

Mittal, R., and Iaccarino, G. 2005. Immersed boundary methods. *Ann. Rev. Fluids Mech.* 37, 239–261.

Mori, Y., Liu, C., and Eisenberg, R.S. 2011. A model of electrodiffusion and osmotic water flow and its energetic structure. *Phys. D* 240, 1835–1852.

Nonner, W., Catacuzzeno, L., and Eisenberg, B. 2000. Binding and selectivity in L-type calcium channels: A mean spherical approximation. *Biophys. J.* 79, 1976–1992.

Nonner, W., Chen, D.P., and Eisenberg, B. 1998. Anomalous mole fraction effect, electrostatics, and binding in ionic channels. *Biophys. J.* 74, 2327–2334.

Nonner, W., and Eisenberg, B. 1998. Ion permeation and glutamate residues linked by Poisson-Nernst-Planck theory in L-type calcium channels. *Biophys. J.* 75, 1287–1305.

Pan, K., Tan, Y., and Hu, H. 2010. An interpolation matched interface and boundary method for elleptic interface problems. *J. Comput. Appl. Math.* 234, 73–94.

Peskin, C.S. 1977. Numerical analysis of blood flow in the heart. *J. Comput. Phys.* 25, 220–252.

Sagui, C., and Darden, T.A. 1999. Molecular dynamics simulations of biomolecules: Long-range electrostatic effects. *Annu. Rev. Biophys. Biomol. Struct.* 28, 155–179.

Sheng, P., Zhang, J., and Liu, C. 2008. Onsager principle and electrorheological fluid dynamics. *Prog. Theor. Phys.* 175, 131–143.

Shu, C., Ren, W.W., and Yang W.M. 2013. Novel immersed boundary method for thermal flow problems. *Int. J. Numer. Method H.* 23, 124–142.

Xu, X., Liu, C., and Qian, T. 2012. Hydrodynamic boundary conditions for one-component liquid-gas flows on non-isothermal solid substrates. *Commun. Math. Sci.* 10, 1027–1053.

Zheng, Q., and Wei, G-W. 2011. Poisson-Boltzmann-Nernst-Planck Model. *J. Chem. Phys.* 19, 134.

Zhu, Y.C., Zhao, S. Feig, M., et al. 2006. High order matched interface and boundary method for elliptic equations with discontinuous coefficients and singular sources. *J. Comput. Phys.* 1, 1–30.

Address correspondence to:
Prof. Tony W.H. Sheu
Department of Engineering Science and Ocean Engineering
National Taiwan University
Taipei 10617
Taiwan

E-mail: twhsheu@ntu.edu.tw